Carbohydrate Polymers 157 (2017) 38–47

Contents lists available at ScienceDirect

Carbohydrate Polymers

journal homepage: www.elsevier.com/locate/carbpol

Investigation of bio polymer electrolyte based on cellulose acetate-ammonium nitrate for potential use in electrochemical devices

S. Monisha[a,b], T. Mathavan[a], S. Selvasekarapandian[b,*], A. Milton Franklin Benial[a], G. Aristatil[c], N. Mani[c], M. Premalatha[a,b], D. Vinoth pandi[d]

[a] Research Department of Physics, N.M.S.S. Vellaichamy Nadar College, Madurai, Tamil Nadu 625 019, India
[b] Materials Research Center, Coimbatore, Tamil Nadu 641 045, India
[c] Ingsman Energy and Fuel Cell Organization Pvt. Ltd., Chennai, Tamil Nadu 600096, India
[d] Coimbatore Institute of Technology, Cimbatore, Tamil Nadu 641 014, India

ARTICLE INFO

Article history:
Received 10 June 2016
Received in revised form 9 September 2016
Accepted 9 September 2016
Available online 11 September 2016

Keywords:
Biopolymer electrolyte
Proton conduction
Ionic conductivity
DFT calculations
Proton battery
Fuel cell

ABSTRACT

Proton conducting materials create prime interest in electro chemical device development. Present work has been carried out to design environment friendly new biopolymer electrolytes (BPEs) using cellulose acetate (CA) complex with different concentrations of ammonium nitrate (NH_4NO_3), which have been prepared as film and characterized. The 50 mol% CA and 50 mol% NH_4NO_3 complex has highest ionic conductivity (1.02×10^{-3} S cm^{-1}). Differential scanning calorimetry shows the changes in glass transition temperature depends on salt concentration. Structural analysis indicates that the highest ionic conductivity complex exhibits more amorphous nature. Vibrational analysis confirms the complex formation, which has been validated theoretically by Gaussian 09 software. Conducting element in the BPEs has been predicted. Primary proton battery and proton exchange membrane fuel cell have been developed for highest ionic conductivity complex. Output voltage and power performance has been compared for single fuel cell application, which manifests the present BPE holds promise application in electrochemical devices.

1. Introduction

The source of energy from "green materials" has gained significance due to the consequences of global warming and energy crisis. From this green viewpoint, many researchers took effort to develop new biopolymer electrolytes (BPEs). Biopolymer based electrolytes have overcome the main shortcoming of synthetic polymer electrolytes such as high cost and not being environmentally green. Hence, it is imperative to develop BPE in many electrochemical devices such as fuel cell, solar cell, battery, sensors and super capacitors (Ramesh, Liew, & Arof, 2011).

In order to develop environment friendly polymer electrolytes, some of the essential and necessary requirements are membrane with good ionic conductivity, low cost, good dimensional and good mechanical stabilities (Samsudin, Khairul, & Isa, 2012). Natural polymers meet the above requirements so as to use as an electrolyte. Recently, researchers proposed many natural polymers such as cellulose and its derivative (Yue & Cowie, 2002; Yue, McEwen, & Cowie, 2003), starch (Ramesh et al., 2011), chitosan (Shukur, Yusof, Zawawi, Illias, & Kadir, 2013), and carboxylmetylcellulose (Samsudin, Lai, & Isa, 2014), which are suitable to be used as host polymer in the BPEs.

Among the natural polymers, polysaccharide polymer cellulose acetate (CA) has got a number of good quality to process as membrane with good adhesion, an excellent transparency, non-toxic nature, low cost, biodegradable and biocompatible (Daniel Cerqueira, Artur Valente, Guimes Filho, & Hugh Burrows, 2009; Xiao et al., 2004). Due to this ability, CA has been studied intensely for various applications (Chou, Yu, Yang, & Jou, 2007; Edgar et al., 2001). Additionally, it contains anionic polysaccharide in its backbone, which has high affinity towards proton ions. The main limitation of CA has been attributed to its high crystalline nature, which gives the lowest ionic conductivity of order 10^{-7} S cm^{-1}. To overcome the above limitation, natural polymer CA has been doped with ammonium salts like ammonium thiocyanate (NH_4SCN) (Monisha et al., 2016; Woo, Majid, & Arof, 2012), ammonium nitrate (NH_4NO_3)

* Corresponding author.
E-mail address: sekarapandian@rediffmail.com (S. Selvasekarapandian).

http://dx.doi.org/10.1016/j.carbpol.2016.09.026
0144-8617/

(Kadir, Aspanut, Majid, & Arof, 2011), and ammonium iodide (NH_4I) (Kumar, Tiwari, & Srivastava, 2012), which provide ions for conduction. Ammonium salts are chosen because it is considered as good proton donor to the polymer matrix (Chandra, Hashmi, & Prasad, 1990; Kumar & Sekhon, 2002). Daniel et al. found that in the polyethylene oxide (PEO)-ammonium hydrogen sulphate (NH_4HSO_4) and poly(acrylic acid) (PAA)-NH_4HSO_4 electrolytes anions were practically immobile and NH_4^+ cations were the dominant charge carriers (Daniel, Desbat, & Lassegues, 1998). Previous Researchers (Abidin, Ali, Hassan, & Yahya, 2013; Ramesh, Shanthi, & Morris, 2012; Ramesh, Shanthi, & Morris, 2013; Selvakumar & Krishna Bhat, 2008) have developed CA membrane using lithium salts. Recently, cellulose and its derivatives have been successfully employed in Li-ion batteries for the production of electrodes, separators or as reinforcing agents in gel polymer or solid polymer electrolytes. Cellulose based Li-ion batteries are well reviewed by Jabbour et al. (Jabbour, Bongiovanni, Chaussy, Gerbaldi, & Beneventi, 2013). Weng et al. investigated the use of fibrous cellulose membrane for developing the separators for high performance lithium ion batteries (Weng, Xu, Alcoutlabi, Mao, & Lozano, 2015). A cellulose based composite nonwoven has been explored as lithium ion battery separator by Zhang et al: The cell using the composite separators displayed better rate capability and enhanced capacity retention, which is compared to those of commercialized polypropylene separator (Zhang et al., 2013).

Harun et al. reported that the dielectric behavior of CA complexes with ammonium tetrafluroborate (NH_4BF_4) and polyethyleneglycol (PEG) (Harun, Ali, Ali, & Yahya, 2012), which suggest that CA-NH_4BF_4 film has conductivity of 2.18×10^{-7} S cm^{-1} and it enhanced to 1.41×10^{-5} S cm^{-1} with addition of 30 wt% of PEG. Johari et al. carried out a study on CA based gel polymer electrolytes and reported the ionic conductivity, which was found to be 10^{-2} S cm^{-1} (Johari, Kudin, Ali, Winie, & Yahya, 2009; Johari, Kudin, Ali, & Yahya, 2009). However, one of the drawbacks of this gel polymer electrolyte is the lack of long-term structural stability, which causes a reduction of the contact area with the electrode and a resultant fall in conductance (Quartarone, Tomasi, Mustarelli, Appetecchib, & Croceb, 1998). Indeed, solid BPE is capable of operating as thin films of desirable size, satisfactory mechanical properties and good contact with electrode materials (Winie, Ramesh, & Arof, 2009). Literature survey reveals that the proton transport studies of CA based polymer complexes are scarce.

In this communication, we study the biopolymer CA doped with different concentration of NH_4NO_3 and it has been characterized by various techniques namely, ionic conductivity, thermal properties, structural conversion and complexation. The infrared spectrum has been simulated theoretically and validated by experimentally recorded spectrum, which gives deep understanding on the complex formation of BPE system. The potential of highest proton conducting BPE as an electrolyte system in battery has also been studied. A new proton exchange membrane (PEM) fuel cell has been constructed using highest proton conducting membrane 50CA:50NH_4NO_3. Output voltage and power performance of the fuel cell with 50CA:50NH_4NO_3 membrane is compared with standard nafion 117.

2. Materials and methods

2.1. Materials

Polymer Cellulose Acetate (CA) has been purchased from Sigma Aldrich (Average M_n = 50,000 by GPC, P.Code:1001345528, 419028-500G, lot# MWBK7408V). The salt ammonium nitrate (NH_4NO_3) (M.W = 80.024 g/mol) has been purchased from NICE chemicals private Ltd., Kerala, India. The solvent dimethyl formamide (DMF) (M.W = 73.08 g/mol, density = 0.948–0.949 kg/m^3) has been purchased from Merck specialities private Ltd., Mumbai, India. All the chemicals have been used without any further purification.

The cellulose acetate is crystalline in nature. The crystalline nature of the polymer will be changed due to the addition of NH_4NO_3, which has been confirmed by powder XRD.

2.2. Preparation of biopolymer electrolyte films

CA and NH_4NO_3 complex has been synthesized by solution cast-technique with different concentrations. The CA and NH_4NO_3 complex has been prepared by dissolving CA and NH_4NO_3 in DMF with proper ratios [(90:10), (80:20), (70:30), (60:40), (50:50) and (40:60) (CA:NH_4NO_3)] and stirred continuously until a homogenous solution was obtained. Then the solution has been transferred into petri dish and dried at 60 °C to eliminate the solvent. The obtained film was taken for further characterization.

2.3. Characterization techniques

2.3.1. Electrochemical impedance spectroscopy (EIS)

Impedance analysis has been performed using impedance spectrometer, which is a powerful method for characterizing the ionic conductivity of freshly casted samples. Prior testing, the thickness of the films was measured by using micrometer screw gauge. Then, the films with well known thickness (0.22–0.66 μm) have been sandwiched between two stainless steel blocking electrodes and tested using HIOKI 3532 in the range of 42 Hz–1 MHz with various temperatures from 303 K to 343 K.

2.3.2. Differential scanning calorimetry (DSC)

The thermal stability of the BPEs has been studied using DSC Q20 V4.10 build 122 with a resolution of 0.01 mg. The films were taken in an aluminum pan and heated up to 500 °C with the heating rate of 5 °C/min under controlled air atmosphere and the films were purged using nitrogen atmosphere during the measurements. Dry nitrogen gas at the rate of 50 ml/min has been purged through the cell during the thermal treatment.

2.3.3. X-ray diffraction (XRD) analysis

The amorphousity of BPE has been investigated using XRD. The XRD patterns of the films were recorded at room temperature by X' pert pro diffractometer system using the Cu-kα radiation in the range of 2θ= 10°–90°.

2.3.4. Fourier transform infrared (FTIR) spectroscopy

The complex formation between the chemical constituents in the CA polymer matrix and the salt has been analyzed by using FTIR. FTIR spectrum of the films was recorded in the wavenumber range 2500–650 cm^{-1} at room temperature using BRUCKER spectrophotometer.

2.3.4.1. Computational details. The molecular structure of CA and CA:NH_4NO_3 complex has been optimized by the DFT/B3LYP method with 6-31G(d,p) basis set using Gaussian 09 program. The IR spectrum of the CA and CA:NH_4NO_3 complex has been simulated. The vibrational assignments have been made by Gauss View 05 program using the animation option. The calculated vibrational frequencies have no imaginary values, which indicates that the optimized molecular structure of CA and CA:NH_4NO_3 complex have been located at the local minimum potential energy surface.

2.3.5. Transference number measurement (TNM)

TNM has been performed using dc polarization method in order to prove the proton conduction in BPEs system. The dc current was

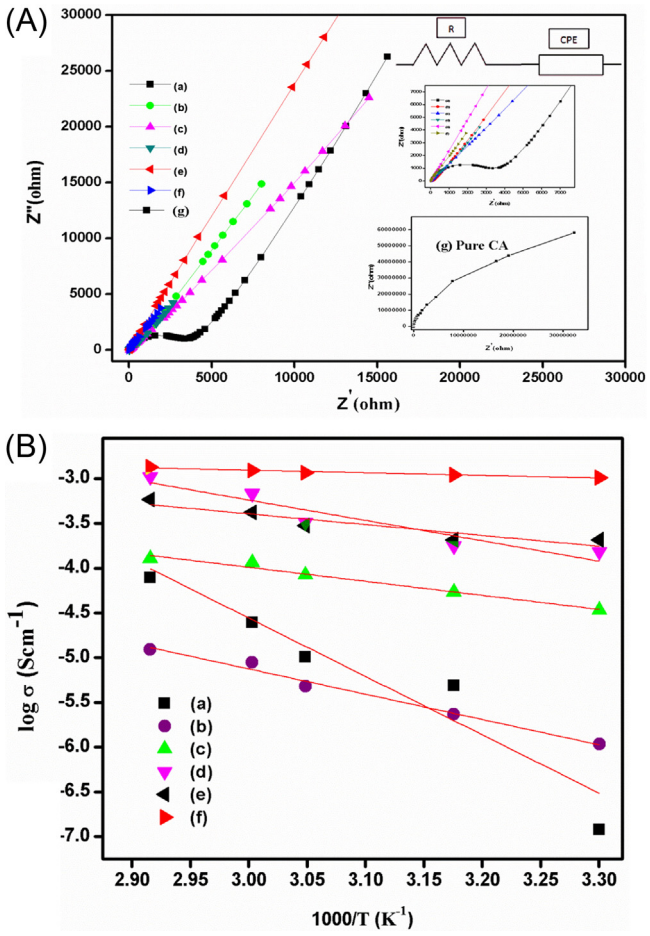

Fig. 1. (A) Cole–Cole plot for (a) 90CA:10NH_4NO_3, (b) 80CA:20NH_4NO_3, (c) 70CA:30NH_4NO_3, (d) 60CA:40NH_4NO_3, (e) 50CA:50NH_4NO_3, (f) 40CA:60NH_4NO_3, (g) Pure CA BPEs and the corresponding equivalent circuit. (B) Temperature dependence ionic conductivity of (a) Pure CA (b) 90CA:10NH_4NO_3. (c) 80CA:20NH_4NO_3, (d) 70CA:30NH_4NO_3, (e) 60CA:40NH_4NO_3 and (f) 50CA:50NH_4NO_3 BPEs.

monitored as a function of time on the application of fixed dc voltage (1.5 V) across the sample mounted between two stainless steel electrodes.

2.3.6. Fabrication of proton battery and fuel cell

Using the highest conducting BPE 50CA:50NH_4NO_3 a proton battery and a PEM fuel cell have been constructed and their results are discussed.

3. Results and discussion

3.1. Ionic conductivity study

The ionic conductivity of BPEs depends on several factors, such as ionic conducting species, types of charge carriers (cationic or anionic) and the temperature. The evolution of the typical impedance plot (Z′ and Z″) as a function of variation in CA:NH_4NO_3 matrix has been shown in Fig. 1A. In general, the complex impedance plot has high frequency semicircle ascribed to the bulk of polymer electrolytes, whereas the low frequency spike is due to the capacitance of the double-layer formed at the electrode/electrolyte interface (Baskaran, Selvasekarapandian, Kuwata, Kawamura, & Hattori, 2006; Ravi et al., 2011).

From Fig. 1A it has been evidenced from the impedance response behavior, the decrease in the high frequency semicircular portion upon doping NH_4NO_3 from 10 to 50 wt% concludes that the current carriers are ions and the total conductivity, is mainly the result of ion conduction (Jaco, Prabaharan, & Radhakrishna, 1997). The equivalent circuit has been shown in Fig. 1A. EIS parameters have been obtained by using EQ software program developed by Boukamp (1986a, 1986b), where the resistance value of pure CA was obtained as $61.2 \times 10^3\ \Omega$, whereas for 10–50 mol% of NH_4NO_3 doped with CA polymer electrolyte the value of resistance has decreased from 3646 Ω to 17.1 Ω. The constant phase element (CPE) value for pure CA was obtained as $2.66 \times 10^4\ \mu F$. The NH_4NO_3 doped with CA polymer electrolyte have CPE values in the range of 0.0049 to 8.01 μF. The highest conductivity polymer electrolyte 50CA:50NH_4NO_3 has R_b = 17.1 Ω and CPE = 8.01 μF.

The ionic conductivity (σ) of the polymer electrolytes is calculated using the equation,

$$\sigma = \frac{L}{A \times R_b} S\,cm^{-1}$$

where L is the thickness, R_b is the bulk resistance and A is the contact area of the electrolyte film. Table 1 indicates the calculated ionic conductivity for different concentration of CA:NH_4NO_3 BPEs with various temperature. Table 1 illustrates that the ionic conductivity increases with increase in NH_4NO_3 and attains a maximum value of 1.024×10^{-3} at room temperature for 50CA:50NH_4NO_3, which has greater ionic conductivity than that of pure CA ($1.285 \times 10^{-7}\ S\,cm^{-1}$). The observed maximum conductivity value in the present study was higher than the value ($1.41 \times 10^{-5}\ S\,cm^{-1}$) reported by Harun et al. for CA-NH_4BF_4-PEG at room temperature (Harun et al., 2012). The increase in conductivity is due to the changes in mobility and carrier concentration. Further, the enhancement in ionic conductivity is attributed to the increase in the concentration of amorphous phase upon the disruption of bonding between the oxygen (O) and acetate (Ac) atom in −OAc functional group in CA. This allows greater availability of vacant oxygen to assist the proton ions (H^+) mobility by forming temporary ionic interaction. This interaction aids the continuous hopping of H^+ ions from one vacant site to another and thus enhances the ionic conductivity (Uma, Mahalingam, & Stimming, 2003). As observed from Fig. 1A, it has been worth mentioning that above 50 wt% NH_4NO_3 loading, the ionic conductivity decreases. The ionic conductivity value for BPE 40CA:60NH_4NO_3 has been found to be 7.64×10^{-4}. This might be due to decrease in mobility, which could probably be the net effect of the interplay of increasing disorder and viscosity on account of large amount of salt, which has been supported by the literature (Samsudin et al., 2014).

3.2. Temperature dependant conductivity

The temperature-dependant study has been used to analyze the possible mechanism of ionic conduction in BPE system, which follows a linear trend of Arrhenius behavior governed by,

$$\sigma = \sigma_0 \exp\left(-E_a/KT\right)$$

where σ, σ_0, E_a, K and T are the ionic conductivity, pre-exponential factor, activation energy, Boltzmann constant and absolute temperature respectively. Fig. 1B reveals Arrhenius plot for various concentrations of NH_4NO_3 in the BPEs from room temperature to 70 °C. As the temperature increases, the polymer can expand easily and produce free volume. Thus, ions, solvated molecules or polymer segments can move into the free volume. This can be interpreted by “hopping mechanism” between co-ordination sites in which, hopping being assist ion transport and compensate the retarding effect of the ion clouds (Rajendran, Mahendran, & Kannan, 2002). The values of conduction and activation energy as a function of NH_4NO_3 concentration were listed in Table 1, which shows that the activation energy gradually decreases with increase in NH_4NO_3

Table 1
Ionic conductivity and activation energy values of CA:NH_4NO_3 BPEs for different temperature.

Polymer composition (mol%)	σ_{303k}	σ_{313k}	σ_{323k}	σ_{333k}	σ_{343k}	Activation energy E_a (eV) at room temperature	Regression value
Pure CA	1.29×10^{-7}	8.42×10^{-6}	2.68×10^{-5}	2.47×10^{-5}	7.86×10^{-5}	1.2	0.90
90CA:10NH_4NO_3	1.08×10^{-6}	2.34×10^{-6}	4.79×10^{-6}	8.89×10^{-6}	1.24×10^{-5}	0.56	0.98
80CA:20NH_4 NO_3	3.41×10^{-5}	5.42×10^{-5}	8.42×10^{-5}	1.15×10^{-4}	1.28×10^{-4}	0.46	0.95
70CA:30NH_4 NO_3	1.53×10^{-4}	1.78×10^{-4}	3.26×10^{-4}	6.82×10^{-4}	5.86×10^{-4}	0.30	0.94
60CA:40NH_4 NO_3	2.08×10^{-4}	2.51×10^{-4}	3.00×10^{-4}	4.21×10^{-4}	1.05×10^{-3}	0.24	0.90
50CA:50NH_4 NO_3	1.02×10^{-3}	1.10×10^{-3}	1.16×10^{-3}	1.23×10^{-3}	1.34×10^{-3}	0.05	0.98

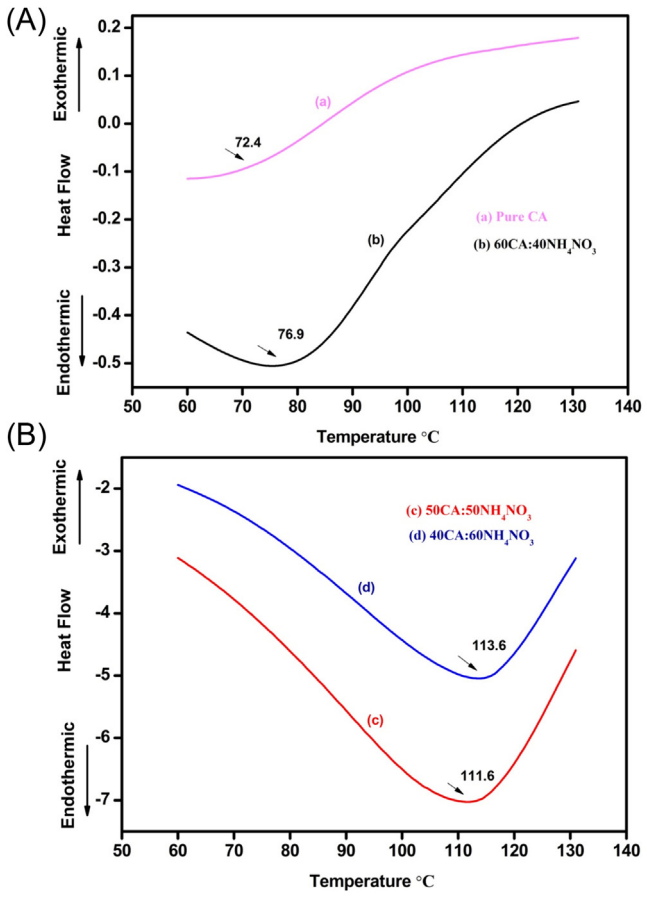

Fig. 2. (A) DSC thermo grams of (a) PURE CA and (b) 60CA:40NH_4NO_3 BPEs. (B) DSC thermo grams of (c) 50CA:50NH_4NO_3 and (d) 40CA:60NH_4NO_3 BPEs.

concentration. The result indicates that not only the number of carriers increases by increasing the NH_4NO_3 concentration, but also the energy barriers are decreased (Kopitzke, Linkous, Anderson, & Nelson, 2000).

3.3. Differential scanning calorimetry (DSC)

The thermal behavior of BPEs has been studied by differential scanning calorimetry technique. From DSC it has been possible to examine the effect of NH_4NO_3 on the thermal transition of CA. Fig. 2A and B shows the DSC thermogram of CA:NH_4NO_3 complexes.

The glass transition temperature (T_g) of BPEs is increased from that of pure CA with increasing NH_4NO_3 ratio upto 40 mol%, which was in agreement with those of Ramesh, Liew, Morris, and Durairaj (2010). From Fig. 2A, the T_g of pure CA has been found to be 72.4 °C, the T_g of 60CA:40NH_4NO_3 has been observed as 76.9 °C, which increased further with increase of NH_4NO_3. Fig. 2B shows that the T_g of 50CA:50NH_4NO_3 has been obtained as 111.6 °C, and the T_g of 40CA:60NH_4NO_3 has been found to be 113.6 °C. According to Fig. 2A and B it is concluded the elevation of T_g is due to the H^+ ions preferring to interact with electron-rich co-ordinating groups, arises from the transient cross-linking bond between H^+ ions and the O atoms in the polymer chains. These cross linkage bonds impede the rotation of polymer segments, leading to stiffening of the polymer chains and hence increase the energy barrier to the segmental movement. Finally, this H^+ and O atoms binding reduces the flexibility of polymer backbone (Li, Yuan, & Yang, 2006; Ramesh and Arof, 2001).

3.4. X-ray diffraction (XRD) analysis

XRD is a versatile tool to monitor the changes in structural properties of both crystalline and amorphous region of BPEs system. Fig. 3A depicts the XRD patterns of pure CA and CA doped with different concentrations of NH_4NO_3. A well known crystalline peaks at $2\theta = 9°$, 18° and 27° have been reported for pure CA film (Ramesh et al., 2013). In order to investigate the influence of salt concentration NH_4NO_3 to pure CA, relative intensity of peak between 9° and 27° has to be evaluated. It is found that relative intensity of peaks decrease with increases in salt content and it seems to be almost flat for 50CA:50NH_4NO_3 [Fig. 3A(c)]. All these information clearly depict that doping salt enhances the amorphous nature in the BPEs system. It has been also noted that NH_4NO_3 doped CA [Fig. 3A(b), A(c) and A(d)] has been free from peaks related to NH_4NO_3, which implies the complete disassociation of NH_4NO_3 salt in CA matrix. This result can be interpreted by Hodge et al. criterion, which establishes a correlation between the intensity of the peak and the degree of crystallinity (Hodge, Edward, & Simon, 1996).

Increase in the amorphous region causes increase in the number of transit sites which improves ionic transport and induces greater ionic conductivity (Hongting, Luo, & Yang, 2007). When more than 40 mol% salt (NH_4NO_3) has been added, the salt gets recrystallize which in turn expected to increase the crystallinity of the BPE as shown in Fig. 3A(d). This leads to decrease the mobile ion and to decrease the conductivity (Samsudin et al., 2012).

3.5. Fourier transform infrared (FTIR) spectroscopy analysis

FTIR analysis has been performed to obtain the structural, compositional and bonding nature of the BPEs system. In FTIR analysis, the occurrence of complexation and interaction between proton ions and oxygen atoms can be deduced in terms of wavenumber shifting, shape, and relative intensity of the IR peaks. In this present investigation FTIR spectral analysis has been performed by both experimentally and theoretically to identify the functional group present in pure CA and CA:NH_4NO_3 complex. Previously Ahmad & Isa reported the FTIR analysis by both experimentally and theoretically for BPEs system (Ahmad & Isa, 2016).

The calculated and observed FTIR vibrational frequencies and corresponding assignments of pure CA and CA:NH_4NO_3 complex has been summarized in Table 2 (Ramesh et al., 2012, 2013) and the FTIR spectrum has been depicted in Fig. 3B. The optimized molec-

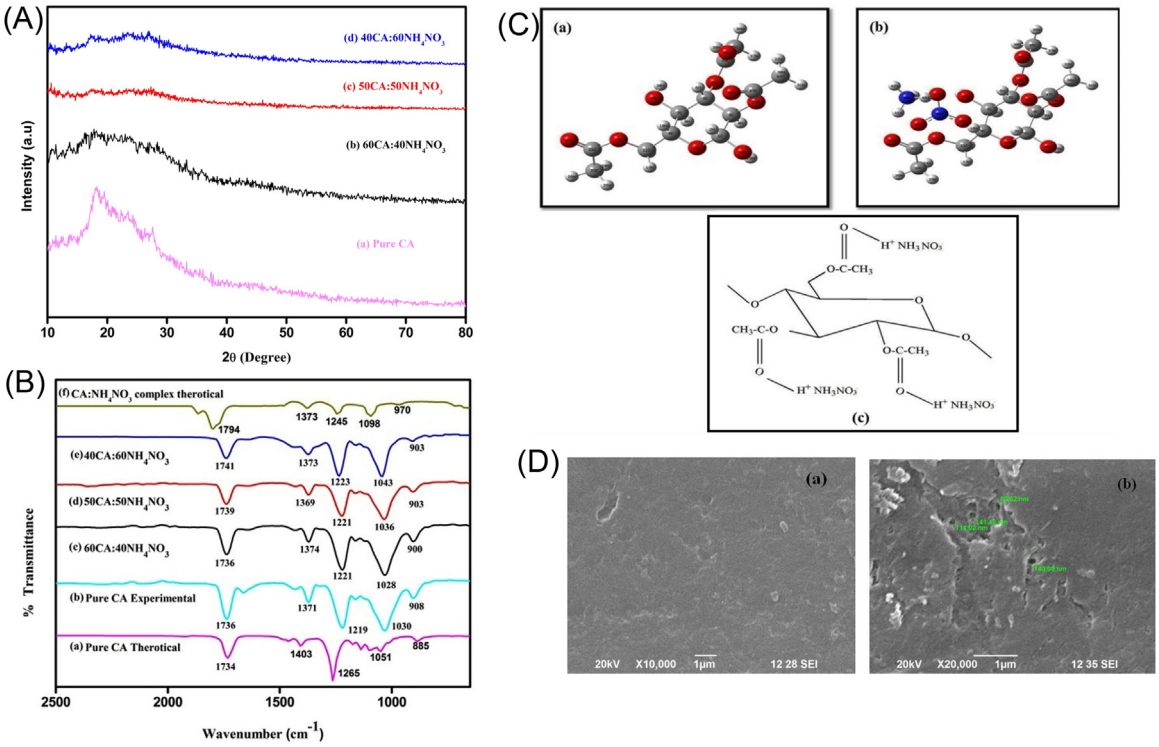

Fig. 3. (A) XRD patterns of (a) pure CA, (b) 60CA:40NH_4NO_3, (c) 50CA:50NH_4NO_3 and (d) 40CA:60NH_4NO_3 BPEs. (B) FTIR spectra of (a) Pure CA theoretical, (b) Pure CA Experimental. (c) 60CA:40NH_4NO_3, (d) 50CA:50NH_4NO_3, (e) 40CA:60NH_4NO_3 and (f) CA:NH_4NO_3 complex theoretical. (C) (a) The optimized molecular structure of pure CA. (b) The optimized molecular structure of CA:NH_4NO_3 complex. (c) Possible interactions between the polymer CA and the dopant NH_4NO_3 BPE. (D) SEM photographs of (a) pure CA, (b) 50CA:50NH_4NO_3.

Table 2
FTIR assignments of the calculated and observed vibrational frequencies of CA:NH_4NO_3 BPEs.

Pure CA Experimental (cm^{-1})	Pure CA Theoretical (cm^{-1})	60CA:40NH_4NO_3 (cm^{-1})	50CA:50NH_4NO_3 (cm^{-1})	40CA:60NH_4NO_3 (cm^{-1})	CA:NH_4NO_3 complex Theoretical (cm^{-1})	Assignments
908	885	900	903	903	970	CH_2 rocking
1030	1051	1028	1036	1043	1098	C—O—C stretching of pyrose ring
1219	1265	1221	1221	1223	1245	C—O stretching
1371	1403	1374	1369	1373	1373	CH_2 in plane bending
1736	1734	1736	1739	1741	1794	C=O symmetric stretching

ular structure of CA and CA:NH_4NO_3 complex has been shown in Fig. 3C(a) and C(b) respectively.

From Fig. 3B, the peak observed at 1736 cm^{-1} has been assigned to C=O stretching vibration of CA (Muddassir, Muhammad, Tahir, & Muhammad, 2011). The absorption peak at 1371 cm^{-1} has been attributed to C—H bending of pure CA. The C—O stretching has been observed at 1219 cm^{-1} for pure CA. The peak observed at 1030 cm^{-1} for pure CA has been assigned to C—O—C stretching of pyrose ring. The medium intensity peak observed at 908 cm^{-1} corresponds to C—H vibrational mode of pure CA. The calculated C=O stretching, CH_2 bending, C—O stretching, C—O—C stretching and CH_2 rocking vibrations of the pure CA have been obtained at 1734, 1403, 1265, 1051 and 885 cm^{-1} respectively, which agree well with the observed values and supported by literature (Ramesh et al., 2012, 2013). The observed FTIR peaks position and intensity (1736, 1371, 1219, 1030 and 908 cm^{-1}) have been shifted due to the addition of 40, 50 and 60 mol% of NH_4NO_3 with CA. Theoretically, the calculated vibrational frequencies for pure CA have been shifted due to the addition of NH_4NO_3, which indicates that the NH_4NO_3 group affects the vibrational mode of pure CA and confirms the complex formation between CA and NH_4NO_3.

Based on previous work (Ahmad & Isa, 2016), it is concluded that the mobile ionic carriers in CA-NH_4NO_3 is one of the loosely bound proton of NH_4^+ ion. Sikkinthar et al. proved that H^+ is the ion serves as a conducting species in polyacrylonitrile (PAN)-ammonium bromide (NH_4Br) sample and the proton conduction for polymer electrolyte film occurs by lone pair migration mechanism or vehicular mechanism (Sikkanthar et al., 2015). The interactions between CA-NH_4NO_3 complexes occurred by one of the four hydrogen atoms in NH_4^+ ions, which can be easily dissociated under the influence of electric field (Hema, Selvasekerapandian, & Hirankumar, 2007). Refer to Fig. 3B, the band assignment at 1371 and 908 cm^{-1} have been affected due to the addition of NH_4NO_3 (Majid & Arof, 2008; Rajeswari, Selvasekarapandian, Sanjeeviraja, Kawamura, & Asath Bahadur, 2014). Since NO_3^- ion is a nucleoplile of negative ion, which seeks electron deficient atom and it makes an interaction with the carbonyl carbon of the polymer chain. Similarly, NH_4^+ cation is an electrophile of positive ion interacts with oxygen atom of C=O group present in pure CA and form intermolecular hydrogen bond, which leads to the wavenumber shift in C=O stretching vibration, which also confirmed and validated by the calculated vibrational frequency values. The possible co-ordination interaction between C=O in CA with H^+ of NH_4NO_3 has been shown in Fig. 3C(c). The FTIR analysis supports the argument that there is a certain amount of electrons withdrawn from (C=O) carbonyl group to form strong hydrogen bonding between CA and NH_4NO_3. Thus,

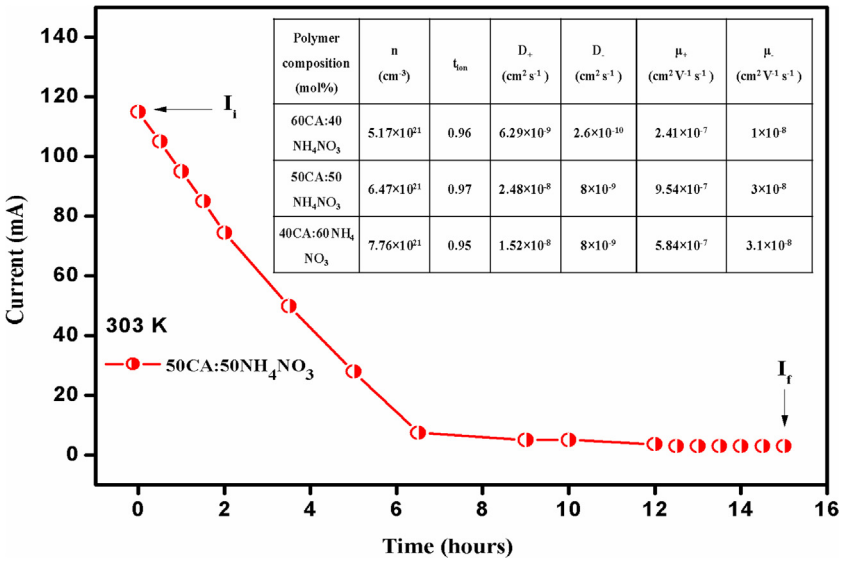

Polymer composition (mol%)	n (cm^{-3})	t_{ion}	D_+ ($cm^2 s^{-1}$)	D_- ($cm^2 s^{-1}$)	μ_+ ($cm^2 V^{-1} s^{-1}$)	μ_- ($cm^2 V^{-1} s^{-1}$)
60CA:40 NH_4NO_3	5.17×10^{21}	0.96	6.29×10^{-9}	2.6×10^{-10}	2.41×10^{-7}	1×10^{-8}
50CA:50 NH_4NO_3	6.47×10^{21}	0.97	2.48×10^{-8}	8×10^{-9}	9.54×10^{-7}	3×10^{-8}
40CA:60 NH_4NO_3	7.76×10^{21}	0.95	1.52×10^{-8}	8×10^{-9}	5.84×10^{-7}	3.1×10^{-8}

Fig. 4. Polarization current vs time plot for 50CA:50NH_4NO_3 BPE and Proton transport properties of CA:NH_4NO_3 BPEs.

FTIR analysis proves the complexation between polymer CA and salt NH_4NO_3 BPE system.

3.6. SEM analysis

The changes in structural morphology of BPE CA:NH_4NO_3 has been determined from the scanned electron micrographs (SEM). Fig. 3D shows the SEM analysis of the surface of pure CA and 50CA:50NH_4NO_3. For pure CA sample Fig. 3D(a), it has been clear that it has uniform surface morphology rather than smooth surface, which indicates that there is no porous formation in the membrane surface.

By adding 50 wt% of salt NH_4NO_3 to pure CA sample, the surface of the film appears to be rough Fig. 3D(b). As seen from Fig. 3D(b), the pores with different size are formed. Porous size is in the range of ~80–250 nm. The photograph of 50CA:50NH_4NO_3 complex with maximum number of pores give rise to high ionic conductivity (Ulaganathan & Rajendarn, 2010). Furthermore, these characteristic lead to a transport mechanism, which have the effective high conductivity and concludes that this type of structure can also improve H^+ transport between the BPE membrane and electrode (Haung & Wunder, 2001). This has been correlated with ionic conductivity data. Finally, the SEM photographs confirm the interaction and complexation between the CA and NH_4NO_3.

3.7. Transference number measurement (TNM)

The transference number measurement (TNM) confirms the nature of particular charge species, whether ions or electrons present in the BPEs system. The measurement of transference number for CA:NH_4NO_3 electrolyte system has been done using Wagner's polarization technique. The results of DC polarization measurement for 50CA:50NH_4NO_3 as a function of time at ambient temperature with fixed DC voltage (1.5 V) has been shown in Fig. 4. The transference number was calculated from the polarization current versus time plot using the equation (Wagner & Wagner, 1957).

$$t_{ion} = (I_i - I_f)/I_i$$

$$t_{elec} = I_f/I_i$$

where I_i is the initial current and I_f is the final residual current. It has been inferred from Fig. 4 the depletion of the charge carriers or ionic species in the electrolyte become constant and causes the initial total current decreases with time. The decreases in the polarization current can be attributed to the migration of ions, which is due to the applied field and balanced by diffusion due to concentration gradient (Muthuvinayagam & Gopinathan, 2015). At a steady state, the cell is polarized and current flows because of the electron migration between the electrolytes and interfaces. Based on Fig. 4, the ionic transference number of the film has been found to be ~0.97. The diffusion coefficients of cations and anions of 60CA:40NH_4NO_3, 50CA:50NH_4NO_3 and 40CA:60NH_4NO_3 were calculated using the following equations (Selvasekarapandian, Hema, Kawamura, Kamishima, & Baskaran, 2010), which were given in Fig. 4.

$$D = D_+ + D_- = \frac{KT\sigma}{ne^2}$$

$$t_+ = \frac{D_+}{D_+ - D_-}$$

The ionic mobility of cations and anions of all the samples are calculated using the following equations.

$$\mu = \mu_+ + \mu_- = \frac{\sigma}{ne}$$

$$t_+ = \frac{\mu_+}{\mu_+ + \mu_-}$$

where e is the charge of the electron, k Boltzmann constant, T absolute temperature, n is the number of charge carriers stochiometrically related to the salt composition, μ_+ and μ_- is the ionic mobility of cation and anion respectively and D_+ and D_- is the diffusion coefficients of cation and anion respectively. From Fig. 4, it has been observed that the values of μ_+ is higher than μ_- and also the values of D_+ is higher than D_- for all BPEs, which indicates that the sample is more cationic (+) than anionic (−) conductor. Highest cationic mobility 9.54×10^{-7} $cm^2 V^{-1} s^{-1}$ has been observed for 50CA:50NH_4NO_3.

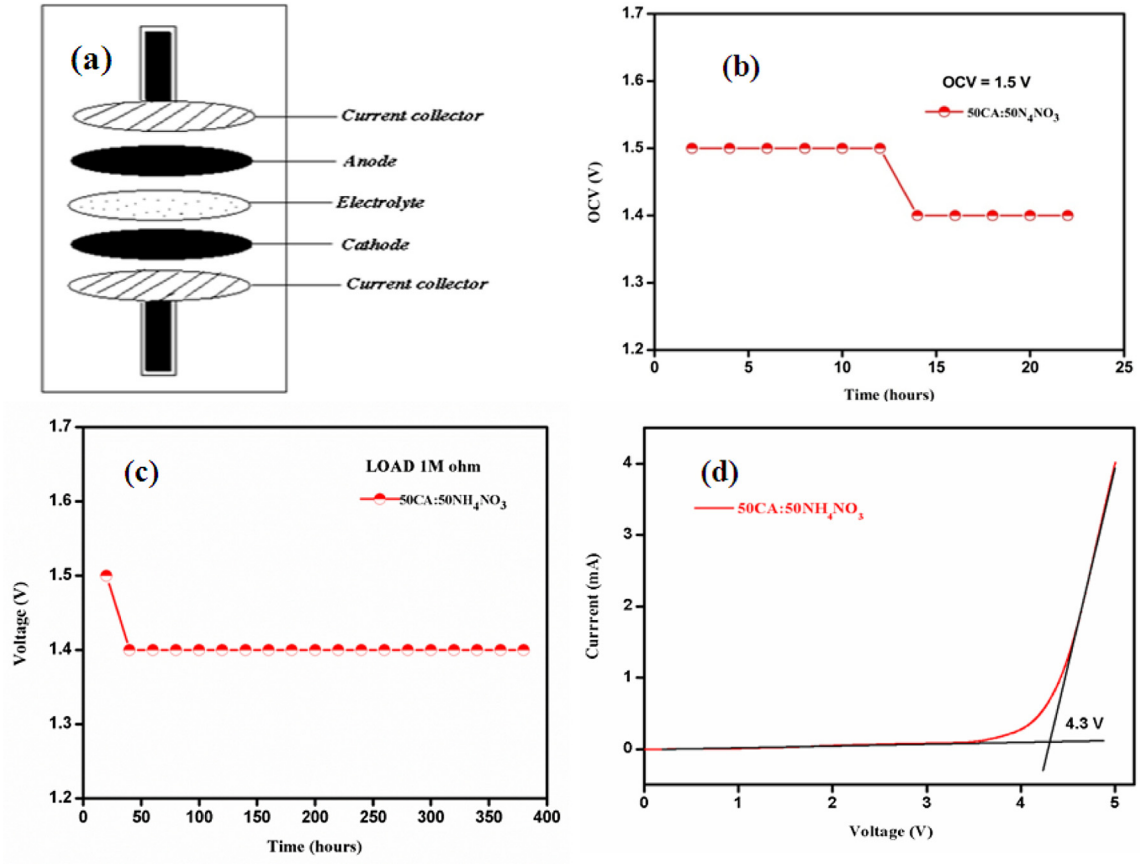

Fig. 5. (a) Schematic diagram of battery configuration. (b) Open circuit voltage as a function of time for 50CA:50NH_4NO_3 BPE. (c) Discharge curves of cell using 1 MΩ for 50CA:50NH_4NO_3 BPE. (d) Linear sweep voltammetry for 50CA:50NH_4NO_3 BPE.

3.8. Fabrication and characterization of proton battery

The highest ionic conductivity with the configuration of Zn + $ZnSO_4 \cdot 7H_2O$/50CA:50NH_4NO_3/PbO_2ZnSO$_4 \cdot 7H_2O$/50CA:50NH_4NO_3/PbO_2 + V_2O_5 was used to fabricate the proton battery. For the battery anode, Zn (Merck Co.) and $ZnSO_4 \cdot 7H_2O$ (Merck Co.) were mixed together and pressed with of 5 ton pressure to form pellet. The same procedure has been done for the cathode comprises of PbO_2 (Loba chemie), V_2O_5 (Loba chemie) and CA:NH_4NO_3 BPE solution. Graphite was added during the preparation of cathode and anode to introduce the electronic conductivity. The highest conducting CA:NH_4NO_3 BPE was sandwiched between anode and cathode in Teflon battery. The schematic diagram of fabricated battery was shown in Fig. 5(a).

The anode and cathode reactions are given below.

Anode reaction

$$nZn + ZnSO_4 \cdot 7H_2O \rightleftarrows Zn_{n+1}(SO_4) \cdot (7-2n)H_2O \cdot 2n(OH) + 2nH^+ + 2ne^-$$

Cathode reaction

$$PbO_2 + 4H^+ + 2e^- \rightleftarrows Pb^{2+} + 2H_2O$$

$$V_2O_5 + 6H^+ + 2e^- \rightleftarrows 2VO^{2+} + 3H_2O$$

Fig. 5(b) shows the open circuit voltage (OCV) of the cell as a function of time at room temperature. The OCV characteristic of the cell at room temperature shows the initial voltage of 1.5 V, dropping to ~1.39 V in the first 11 h of assembly. The cell voltage has been observed to have stabilized and the OCV remained constant at 1.39 V for a period of 8 h. The intermediate drop in the voltage of the cell after fabrication has been due to the cell formation reaction at the electrodes. Similar OCV was reported by Johari et al., for CA based gel polymer electrolyte (Johari, Kudin, Ali, Winie et al., 2009). A dense cellulose based gel polymer electrolyte has been first demonstrated by Li et al., while the use of gel polymer electrolyte shows good electrochemical performance that leads to a low cost, renewable and environment friendly electrolyte for lithium ion batteries (Li et al., 2015).

Fig. 5(c) depicts the discharge characteristic of fabricated proton battery for 50CA:50NH_4NO_3 at room temperature, by connecting it to an external load 1 MΩ. In BPE system, the initial sharp decrease in voltage of this cell may be due to the activation polarization. The activation polarization occurred because the rate of an electrochemical reaction at an electrode surface is controlled by sluggish electrode kinetics (Broadhead & Kuo, 2001). While discharging through 1 MΩ load, the cell voltage has been remained constant at 1.4 V for 350 h. The region in which the cell potential reaches flat discharge rate is called "Plateau region". The important cell parameters of highest conducting BPE 50CA:50NH_4NO_3 are given below:

Cellarea—0.895 cm^2, Cellweight—1.284 g, Celldiameter—1 cm, Thickness—0.28 cm

3.9. LSV study

Electrochemical stability window is essential to use the polymer electrolyte in device. The electrochemical stability of 50CA:50NH_4NO_3 has been examined by linear sweep voltamme-

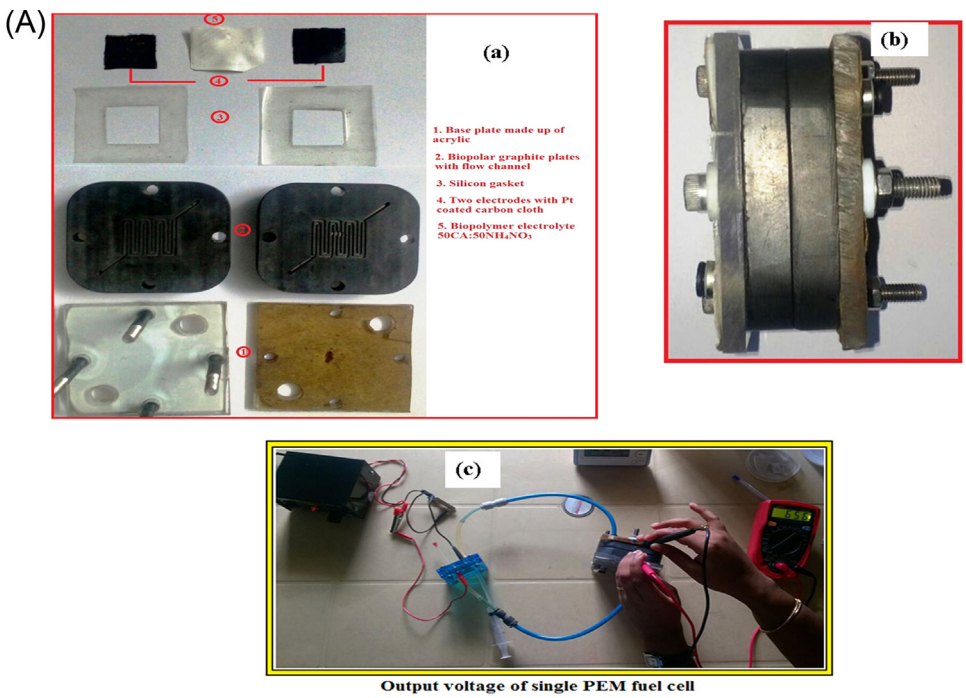

Fig. 6. A(a) Components of single PEM fuel cell. (b) Single PEM fuel cell assembly. (c) Output voltage of single PEM fuel cell. (B) Power performance curve for (a) Standard Nafion 117 (b) BPE 50CA:50NH_4NO_3.

try (LSV) of the cell with two electrode system. Reference and counter electrode are connected together, which acts as one electrode and other as working electrode. So applied voltage has been plotted on the x-axis and the resulting current on the y-axis. The sample has been placed between two stainless steel blocking electrodes using 1 mV s^{-1} scan rate from 0 to 5 V. Fig. 5(d) shows the linear sweep voltammetry curve for 50CA:50NH_4NO_3 at room temperature. The anodic decomposition limit of the polymer electrolyte is considered as the voltage at which the current flows through the cells (Tiankhoon, Ataollahi, Hassan, & Ahmad, 2015). As seen from the plot of current versus voltage the electrolyte shows the electrochemical stability window of 4.3 V. Hence, this BPE is compatible for application in proton battery and electrochemical devices. Abidin et al. also reported approximately the same value of 4.7 V electrochemical stability for γ-butyrolactone (GBL)-0.8 M lithium bis(oxalate) borate (LiBOB)-2 wt% CA (Abidin et al., 2013).

3.10. Construction of single PEM fuel cell

The cell consists of bipolar graphite plates with parallel flow channel size of 7.84 cm^2 and mounted on the two base plates, which is made up of acrylic. A silicon gasket is placed between the two graphite plates. The positive electrode (cathode) and negative electrode (anode) made up of carbon cloth of area ~8.41 cm^2 are coated with Pt at a uniform rate of 0.15 mg/cm. The Pt coated carbon cloth (electrodes) which act as catalyst layer are kept on the either side of flow channel. The highest proton conducting membrane 50CA:50NH_4NO_3/Nafion 117 is sandwiched between the two electrodes. The single PEM fuel cell has been assembled with the above mentioned configuration and is shown in Fig. 6A(a) and A(b). Using a small electrolyzer operated by a voltage of 3 V is used to produce hydrogen and oxygen gas separately. The hydrogen gas with flow rate of 10 ml/min and oxygen gas at a rate of 8 ml/min are passed through the single fuel cell. The anode and the cathode reaction for a PEM fuel cell are given in below equations:

Anode Reaction : $2H_2 \rightarrow 4H^+ + 4e^-$

Cathode Reaction : $O_2 + 4H^+ + 4e^- \rightarrow 2H_2O$

Overall Cell Reaction : $2H_2 + O_2 \rightarrow 2H_2O$

Standard Nafion 117 membrane is placed in constructed fuel cell and a voltage of 900 mV is obtained. Afterwards highest conducting polymer membrane 50CA:50NH_4NO_3 is placed in fuel cell kit and a voltage 656 mV is observed and it is shown in Fig. 6A(c).

A comparison of the PEM fuel cell performance have been recorded using same type of anode and cathode with different flow rate of 400 ml/min for hydrogen gas and 100 ml/min for oxygen gas. The depicted polarization curve for 50CA:50NH_4NO_3 and standard Nafion 117 at 60 °C is shown in Fig. 6B. The single PEM fuel cell performance for standard Nafion 117 displays a current density of 1901 mA/cm^2 at a potential of 60 mV. The power density is observed to be 414 mW/cm^2. Under the same operating conditions, the PEM fuel cell test for 50CA:50NH_4NO_3 displays a current density of 72 mA/cm^2 at a potential of 70 mV, with an accompanying power density of 12 mW/cm^2. The data suggest that the power density of our BPE is lower than Nafion based one. Further, the power performance of our BPE can be enhanced by optimizing the parameters in membrane electrode assembly (MEA) fabrication.

4. Conclusion

The discovery of new BPEs based on CA doped with various concentrations (0–60 wt%) of NH_4NO_3 have been prepared by solution casting technique. A superior ionic conductivity 1.024×10^{-3} has been achieved for the sample 50CA:50NH_4NO_3 at room temperature. The enhancement in mobility of proton ions and flexible structure are responsible for the improvement of ionic conductivity. The rate of increase of ionic conductivity with temperature exhibits Arrhenius behavior where the samples conductivity exclusively affected by temperature and composition of NH_4NO_3. The thermal profile shows the marked increase in T_g, which is an indication of interaction between H^+ ion and carboxyl group of BPEs. Structural and complexation of the BPEs has been ascertained by XRD and FTIR analyses. XRD analysis displays a structural disorderliness of reduced intensity, which concludes the BPE are predominantly amorphous in nature. FTIR and Gaussian results provide an insight into possible co-ordination of interactions between CA and NH_4NO_3. The charge transport in these BPEs has been examined using Wagner's polarization technique and the dominant conducting species are found to be ions rather than electrons. Thus, the optimized BPE 50CA:50NH_4NO_3 with high ionic conductivity has been applied for primary proton battery and PEM fuel cell application, in which their main parameters and output voltage were reported. In spite of extensive research efforts worldwide, power performance of our new polymer membrane 50CA:50NH_4NO_3 has to be optimized and it could satisfactorily replace Nafion. All these result suggest and believe that BPE CA:NH_4NO_3 may offer attractive membrane for electrochemical devices such as proton batteries and fuel cell because of its high performance, eco-friendly, economically cheap and naturally abundant.

References

Abidin, S. Z. Z., Ali, A. M. M., Hassan, O. H., & Yahya, M. Z. A. (2013). Electrochemical studies on cellulose acetate-LiBOB polymer gel electrolytes. *International Journal of Electrochemical Science*, *8*, 7320–7326.

Ahmad, N. H., & Isa, M. I. N. (2016). Characterization of un-plasticized and propylene carbonate plasticized carboxymethyl cellulose doped ammonium chloride solid biopolymer electrolytes. *Carbohydrate Polymers*, *137*, 426–432.

Baskaran, R., Selvasekarapandian, S., Kuwata, N., Kawamura, J., & Hattori, T. (2006). ac impedance, DSC and FT-IR investigations on (x)PVAc–(1-x)PVdF blends with $LiClO_4$. *Materials Chemistry and Physics*, *98*, 55–61.

Boukamp, B. A. (1986a). *Solid State Ionics*, *20*, 301.

Boukamp, B. A. (1986b). *Solid State Ionics*, *18 & 19*, 136.

Broadhead, J., & Kuo, H. C. (2001). In D. Linden, & T. B. Reddy (Eds.), *Handbook of batteries* (p. 2.1). New York: McGraw-Hill.

Chandra, S., Hashmi, S. A., & Prasad, G. (1990). *Solid State Ionics*, *40/41*, 651.

Chou, W. L., Yu, D. G., Yang, M. C., & Jou, C. H. (2007). Effect of molecular weight and concentration of PEG additives on morphology and permeation performance of cellulose acetate hollow fibers. *Separation and Purification Technology*, *57*, 209–219.

Daniel Cerqueira, A., Artur Valente, J. M., Guimes Filho, R., & Hugh Burrows, D. (2009). Synthesis and properties of polyaniline-cellulose acetate blends: The use of sugarcane bagasse waste and the effect of the substitution degree. *Carbohydrate Polymers*, *78*, 402–408.

Daniel, M. F., Desbat, B., & Lassegues, J. C. (1998). Solid state protonic conductors: Complexation of poly(ethylene oxide) or poly(acrylic acid) with NH_4HSO_4. *Solid State Ionics*, *28–30*, 632–636.

Edgar, K. J., Buchanan, C. M., Debenham, J. S., Rundquist, P. A., Seiler, B. D., Shelton, M. C., et al. (2001). Advances in cellulose ester performance and application. *Progress in Polymer Science*, *26*, 1605–1688.

Harun, N. I., Ali, R. M., Ali, A. M. M., & Yahya, M. Z. A. (2012). Dielectric behavior of cellulose acetate based polymer electrolytes. *Ionics*, *18*, 599–606.

Haung, H., & Wunder, S. L. (2001). Preparation of microporous PVDF based polymer electrolytes. *Journal of Power Source*, 649–653.

Hema, M., Selvasekerapandian, S., & Hirankumar, G. (2007). Vibrational and impedance spectroscopic analysis of poly(vinyl alcohol)-based solid polymer electrolytes. *Ionics*, *13*, 483–487.

Hodge, R. M., Edward, G. H., & Simon, G. P. (1996). Water absorption and states of water in semicrystalline poly(vinyl alcohol) films. *Polymer*, *37*, 1371–1376.

Hongting, P. U., Luo, M., & Yang, Z. (2007). Transparent and anhydrous proton conductors based on PVA/imidazole/$NH_4H_2PO_4$ composites. *European Polymer Journal*, *43*, 5076–5083.

Jabbour, L., Bongiovanni, R., Chaussy, D., Gerbaldi, C., & Beneventi, D. (2013). Cellulose-based Li-ion batteries: A review. *Cellulose*, *4*, 1523–1543.

Jaco, M. M. E., Prabaharan, S. R. S., & Radhakrishna, S. (1997). *Solid State Ionics*, *104*, 267–276.

Johari, N. A., Kudin, T. I. T., Ali, A. M. M., Winie, T., & Yahya, M. Z. A. (2009). Studies on cellulose acetate-based gel polymer electrolytes for proton batteries. *Material Research Innovation*, *13*, 232–234.

Johari, N. A., Kudin, T. I. T., Ali, A. M. M., & Yahya, M. Z. A. (2009). Electrochemical studies of composite cellulose acetate-based polymer gel electrolytes for proton. *Proceedings of the National Academy of Sciences Section A Physical Sciences*, *82*, 49–52.

Kadir, M. F. Z., Aspanut, Z., Majid, S. R., & Arof, A. K. (2011). FTIR studies of plasticized poly(vinyl alcohol)-chitosan blend doped with NH_4NO_3 polymer electrolyte membrane. *Spectrochimica Acta Part A: Molecular and Biomolecular Spectroscopy*, *78*, 1068–1074.

Kopitzke, R. W., Linkous, C. A., Anderson, H. R., & Nelson, G. L. (2000). Conductivity and water uptake of aromatic-based proton exchange membrane electrolytes. *Journal of the Electrochemical Society*, *106*, 1677–1681.

Kumar, M., & Sekhon, S. S. (2002). Role of plasticizer's dielectric constant on conductivity modification of PEO–NH_4F polymer electrolytes. *European Polymer Journal*, *38*, 1297–1304.

Kumar, M., Tiwari, T., & Srivastava, N. (2012). Electrical transport behaviour of bio-polymer electrolyte system: Potato starch + ammonium iodide. *Carbohydrate Polymers*, *88*, 54–60.

Li, M. X., Wang, X. W., Yang, Y. Q., Chang, Z., Wu, Y. P., & Holze, R. (2015). A dense cellulose-based membrane as a renewable host for gel polymer electrolyte of lithium ion batteries. *Journal of Membrane Science*, *15*, 112–118.

Li, W., Yuan, M., & Yang, M. (2006). Dual-phase polymer electrolyte with enhanced phase compatibility based on poly(MMA-g-PVC)/PMMA. *European Polymer Journal*, *42*, 1396–1402.

Majid, S. R., & Arof, A. K. (2008). FTIR studies of chitosan-orthophosphoric acid-ammonium nitrate aluminosilicate polymer electrolyte. *Molecular Crystal and Liquid Crystal*, *484*, 117–126.

Monisha, S., Selvasekarapandian, S., Mathavan, T., Milton Franklin Benia, A., Sindhuja, M., & Karthikeyan, S. (2016). Preparation and characterization of biopolymer electrolyte based on cellulose acetate for potential applications in energy storage devices. *Journal of Materials Science Materials in Electronics*, http://dx.doi.org/10.1007/s10854-016-4971-x

Muddassir, A., Muhammad, Z., Tahir, J., & Muhammad, T. Z. B. (2011). Influence of glycol additives on the structure and performance of cellulose acetate/zinc oxide blend electrolytes. *Desalination*, *270*, 98–104.

Muthuvinayagam, M., & Gopinathan, C. (2015). Characterization of proton conducting polymer blend electrolytes based on PVdF-PVA. *Polymer*, *68*, 122–130.

Quartarone, E., Tomasi, C., Mustarelli, P., Appetecchib, G. B., & Croceb, F. (1998). Long term structural stability of PMMA-based gel polymer electrolytes. *Electrochimica Acta*, *43*, 1435–1439.

Rajendran, S., Mahendran, O., & Kannan, R. (2002). Ionic conductivity studies in composite solid polymer electrolytes based on methylmethacrylate. *Journal of Physics and Chemistry of Solids*, *63*, 303–307.

Rajeswari, N., Selvasekarapandian, S., Sanjeeviraja, C., Kawamura, J., & Asath Bahadur, S. (2014). A study on polymer blend electrolyte based on PVA/PVP with proton salt. *Polymer Bulletin*, *71*, 1061–1080.

Ramesh, S., & Arof, A. K. (2001). Structural, thermal and electrochemical cell characteristics of poly(vinyl chloride)-based polymer electrolytes. *Journal of Power Sources*, *99*, 41–47.

Ramesh, S., Liew, C.-W., & Arof, A. K. (2011). Ion conducting corn starch biopolymer electrolytes doped with ionic liquid 1-butyl-3-methylimidazolium hexafluorophosphate. *Journal of Non-Crystalline Solids*, *357*, 3654–3660.

Ramesh, S., Liew, C.-W., Morris, E., & Durairaj, R. (2010). Effect of PVC on ionic conductivity, crystallographic structural, morphological and thermal characterizations in PMMA–PVC blend-based polymer electrolytes. *Thermochimica Acta*, *511*, 140–146.

Ramesh, S., Shanthi, R., & Morris, E. (2012). Plactizing effect of 1-allyl-3-methylimidazolium chloride in cellulose acetate based polymer electrolytes. *Carbohydrate Polymers*, *87*, 2624–2629.

Ramesh, S., Shanthi, R., & Morris, E. (2013). Characterization of conducting cellulose acetate based polymer electrolytes doped with green ionic mixture. *Carbohydrate Polymer*, *9*, 14–21.
Ravi, M., Pavani, Y., Kiran Kumar, K., Bhavani, S., Sharma, A. K., & Narasimha Rao, V. V. R. (2011). Studies on electrical and dielectric properties of PVP:KBrO4 complexed polymer electrolyte films. *Materials Chemistry and Physics*, *130*, 442–448.
Samsudin, A. S., Khairul, W. M., & Isa, M. I. N. (2012). Characterization on the potential of carboxy methylcellulose for application as proton conducting biopolymer electrolytes. *Journal of Non-Crystalline Solids*, *358*, 1104–1112.
Samsudin, A. S., Lai, H. M., & Isa, M. I. N. (2014). Biopolymer materials based carboxymethyl cellulose as a proton conducting biopolymer electrolyte for application in rechargeable proton battery. *Electrochimica Acta*, *129*, 1–13.
Selvakumar, M., & Krishna Bhat, D. (2008). $LiClO_4$ doped cellulose acetate as biodegradable polymer electrolyte for supercapacitors. *Journal of Applied Polymer Science*, *110*, 594–602.
Selvasekarapandian, S., Hema, M., Kawamura, J., Kamishima, O., & Baskaran, R. (2010). Characterization of PVA-NH_4NO_3 polymer electrolyte and its application in rechargeable proton battery. *Journal of the Physical Society of Japan*, *79*(Suppl. A), 163–168.
Shukur, M. F., Yusof, Y. M., Zawawi, S. M. M., Illias, H. A., & Kadir, M. F. Z. (2013). Electrical analysis of amorphous corn starch-based polymer electrolyte membranes doped with LiI. *Physica Scripta*, *88*(10) http://dx.doi.org/10.1088/0031-8949/2013/T157/014050
Sikkanthar, S., Karthikeyan, S., Selvasekarapandian, S., Vinoth Pandi, D., Nithya, S., & Sanjeeviraja, C. (2015). Electrical conductivity characterization of polyacrylonitrile-ammonium bromide polymer electrolyte system. *Journal of Solid State Electrochemistry*, *19*, 987–999.
Tiankhoon, L., Ataollahi, N., Hassan, N. H., & Ahmad, A. (2015). Studies of porous solid polymeric electrolytes based on poly(vinylidene fluoride) and poly(methyl methacrylate) grafted natural rubber for applications in electrochemical devices. *Journal of Solid State Electrochemistry*, http://dx.doi.org/10.1007/s10008-015-3017-2
Ulaganathan, M., & Rajendarn, S. (2010). Preparation and characterizations of PVAc/P(VdF-HFP)-based polymer blend electrolytes. *Ionics*, *16*, 515–521.
Uma, T., Mahalingam, T., & Stimming, U. (2003). Mixed phase solid polymer electrolytes based on poly(methylmethacrylate). *Materials Chemistry and Physics*, *82*, 478–483.
Wagner, J. B., & Wagner, C. J. (1957). Electrical conductivity measurements on cuprous halides. *Journal of Chemical Physics*, *26*, 1597.
Weng, B., Xu, F., Alcoutlabi, M., Mao, Y., & Lozano, K. (2015). Fibrous cellulose membrane mass produced via forcespinning® for lithium-ion battery separators. *Cellulose*, *2*, 1311–1320.
Winie, T., Ramesh, S., & Arof, A. K. (2009). Studies on the structure and transportproperties of hexanoyl chitosan-based polymer electrolytes. *Physica B*, *404*, 4308–4311.
Woo, H. J., Majid, S. R., & Arof, A. K. (2012). Dielectric properties and morphology of polymer electrolyte based on poly(ε-caprolactone) and ammonium thiocyanate. *Materials Chemistry and Physics*, *134*, 755–761.
Xiao, D., Hu, J., Zhang, M., Li, M., Wang, G., & Yao, H. (2004). Synthesis and characterization of camphorsulfonyl acetate of cellulose. *Carbohydrate Research*, *339*, 1925–1931.
Yue, Z., & Cowie, J. M. G. (2002). Synthesis and characterization of ion conducting cellulose esters with PEO side chains. *Polymer*, *43*, 4453–4460.
Yue, Z., McEwen, I. J., & Cowie, J. M. G. (2003). Novel gel polymer electrolytes based on a cellulose ester with PEO side chains. *Solid State Ionics*, *156*, 155–162.
Zhang, J., Liu, Z., Kong, Q., Zhang, C., Pang, S., Yue, L., et al. (2013). Renewable and superior thermal-resistant cellulose-based composite nonwoven as lithium-ion battery separator. *ACS Applied Materials & Interfaces*, *5*, 128–134.